Journal of Magnetic Resonance 194 (2008) 254–263

Contents lists available at ScienceDirect

Journal of Magnetic Resonance

journal homepage: www.elsevier.com/locate/jmr

Relaxation-based distance measurements between a nitroxide and a lanthanide spin label

H. Jäger [a], A. Koch [a], V. Maus [a], H.W. Spiess [a], G. Jeschke [b,*]

[a] Max Planck Institute for Polymer Research, Postfach 3148, 55021 Mainz, Germany
[b] Universität Konstanz, Fachbereich Chemie, Universitätsstrasse 10, 78457 Konstanz, Germany

ARTICLE INFO

Article history:
Received 8 January 2008
Revised 15 July 2008
Available online 18 July 2008

Keywords:
EPR
Inversion recovery
Spin labeling
Distance measurement
Relaxation

ABSTRACT

Distance measurements by electron paramagnetic resonance techniques between labels attached to biomacromolecules provide structural information on systems that cannot be crystallized or are too large to be characterized by NMR methods. However, existing techniques are limited in their distance range and sensitivity. It is anticipated by theoretical considerations that these limits could be extended by measuring the enhancement of longitudinal relaxation of a nitroxide label due to a lanthanide complex label at cryogenic temperatures. The relaxivity of the dysprosium complex with the macrocyclic ligand DOTA can be determined without direct measurements of longitudinal relaxation rates of the lanthanide and without recourse to model compounds with well defined distance by analyzing the dependence of relaxation enhancement on either temperature or concentration in homogeneous glassy frozen solutions. Relaxivities determined by the two calibration techniques are in satisfying agreement with each other. Error sources for both techniques are examined. A distance of about 2.7 nm is measured in a model compound of the type nitroxide–spacer–lanthanide complex and is found in good agreement with the distance in a modeled structure. Theoretical considerations suggest that an increase of the upper distance limit requires measurements at lower fields and temperatures.

1. Introduction

Recently, the measurement of distances between nitroxide spin labels by pulsed electron paramagnetic resonance (EPR) techniques [1–5] has found widespread application in studies of structure and dynamics of biomacromolecules and biomacromolecular complexes [6–10]. With commercial hardware and without isotope labeling such methods can routinely access the distance range between 1.8 and 5 nm, which fits well to the size of the target structures. Double-quantum techniques combined with dedicated hardware [4] may allow for an extension to somewhat shorter distances while deuterium exchange of the matrix allows for an extension to longer distances [11–13], in favorable cases up to 8 nm [14]. Good-quality measurements can be performed on samples with spin label concentrations down to about 50 μM. This is sufficient for site-directed spin labeling (SDSL) [15,16] studies of proteins that can be overexpressed, but may be insufficient for some other interesting applications. An extension of the distance range, in particular towards longer distances, would also be advantageous.

The limit of existing techniques towards short distances is set by the excitation bandwidth of the pulses [17,19] while the limit towards long distances and sensitivity are governed by the fact that the resolution of the measurement is related to T_2 of the nitroxide spin label [7]. To optimize resolution constant-time pulse sequences are applied with lengths that significantly exceed T_2. In this situation only a small fraction of the original echo signal is detected. Furthermore, measurements of long distances require low concentrations, as otherwise separation of the wanted intramolecular contribution from the unwanted intermolecular contribution fails [7]. After more than a decade of intense method development all these limits are well explored and the techniques well optimized. Only gradual improvements can be expected in the future.

These considerations suggest to complement existing approaches by measurements based on a different physical principle. Measurements based on relaxation enhancement of a slowly relaxing electron spin by a fast relaxing electron spin [18] do not require that the excitation bandwidth of microwave pulses is comparable to the dipole–dipole coupling between the two spins and do not rely on a long T_2 of the slowly relaxing spin. The signal loss of constant-time techniques is avoided so that these techniques are potentially more sensitive. Metal complex sites, which can serve as fast relaxing spins, can be engineered by SDSL techniques [20,21]. Relaxation-based measurements may thus be well suited for extending the class of accessible target structures.

In fact, measurement of the distance between a slowly and a fast relaxing spin probe in biological objects was suggested already in

* Corresponding author. Fax: +49 7531 88 3139.
E-mail address: Gunnar.Jeschke@uni-konstanz.de (G. Jeschke).

1090-7807/$ - see front matter © 2008 Elsevier Inc. All rights reserved.
doi:10.1016/j.jmr.2008.07.012

the 1970s [22–24], well before the advent of SDSL techniques, multifrequency EPR and fast computers for data analysis. In another series of pioneering papers distances of slowly relaxing paramagnetic centers in a protein from the protein surface were estimated by using homogeneously distributed fast relaxing species [25–27]. The technique was further developed in the 1980s and 1990s [28–32] is continuously applied in studies of metalloproteins at low temperatures [33] and has recently been demonstrated to be feasible at physiological temperatures [34]. In this paper, we explore the potential of similar approaches with current state-of-the-art spectrometers, cryogenics, and computation power for data analysis. We focus on lanthanide complexes as fast relaxing species. Such labels can also be applied in NMR [35] and fluorescence resonance energy transfer (FRET) [36] measurements and can thus act as multiply addressable nanostructure probes that allow for correlation of spatial information on different length scales.

The paper is structured as follows. In Section 3 we provide a short overview of theoretical approaches to relaxation enhancement by a fast relaxing spin that were developed in the contexts of EPR and solid-state NMR experiments. We explain our computational approach for determining a mean relaxivity of a lanthanide complex from measurements of the temperature or concentration dependence of relaxation enhancement in homogeneous frozen solution. In Section 4 we present data on the temperature dependence of the relaxation time of the nitroxide probe TEMPOL in the presence and absence of a dysprosium complex with the macrocyclic ligand DOTA. Furthermore, concentration dependence is studied at three selected temperatures. We demonstrate analysis of relaxation data for a model compound of the type nitroxide–spacer–lanthanide complex with diamagnetic lanthanum and paramagnetic dysprosium as the metal ions. In Section 5 we examine the precision and range of the technique and consider how the measurement protocols can be optimized with respect to the short distance limit, the long distance limit, and sensitivity.

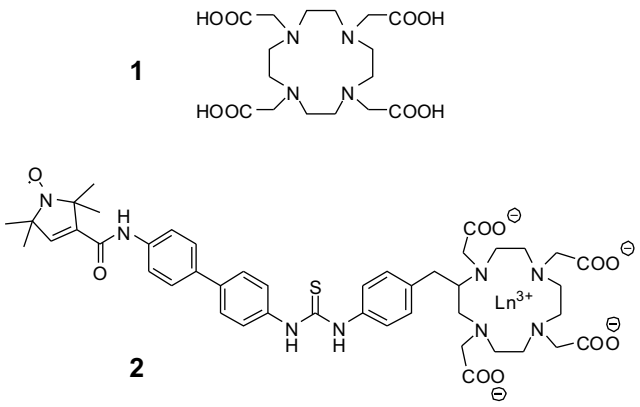

Fig. 1. Structures of lanthanide ligand **1** (1,4,7,10-tetraazacyclododecane-1,4,7,10-tetraacetic acid, DOTA) and model compound **2**. The lanthanide ion Ln^{3+} was either diamagnetic La^{3+} or paramagnetic Dy^{3+}. Note that the lanthanide is coordinated by the four nitrogens and by four oxygen atoms of the carboxylate groups. The ninth coordination position is taken by a water molecule.

2. Materials and methods

2.1. Model systems

Measurements on homogeneous frozen solutions were performed in a mixture of 60% glycerol and 40% water (v/v) that was filled into 3-mm EPR tubes homemade from Herasil tubing and shock-frozen by direct immersion into liquid nitrogen. The concentration of TEMPOL (4-hydroxy-2,2,6,6,-tetramethyl-piperidin-1-oxyl, Aldrich) was kept constant at 250 μM. 1,4,7,10-Tetraazacyclododecane-1,4,7,10-tetraacetic acid (DOTA, Macrocyclics, Dallas, TX) was dissolved in water by adding as much sodium hydrogen carbonate (Aldrich) as was necessary to keep pH neutral (pH = 7). Lanthanum(III) chloride and dysprosium(III)chloride were obtained from Aldrich and were added to the ligand solutions several hours before the measurements to ensure complete complex formation.

The model compound **2** (Fig. 1) was synthesized in two steps as follows:

N-(4′-Amino-biphenyl-4-yl)-2,2,5,5-tetramethyl-1-oxyl-2,5-dihydro-1H-pyrrol-3-carboxamide ***1a****:* 3-Carboxy-2,2,5,5-tetramethyl-3-pyrrolin-1-yloxy (461 mg, 2.50 mmol, Acros), benzidine (155 mg, 0.84 mmol, Aldrich) and 4-(dimethylamino)pyridine (342 mg, 2.80 mmol, Aldrich) were dissolved in tetrahydrofuran (40 ml). While cooling in an ice bath, dicyclohexylcarbodiimide (516 mg, 2.50 mmol, Aldrich) in tetrahydrofuran (20 ml) was added dropwise with a syringe and the mixture stirred overnight. Alternatively, the equivalent amount of diisopropylcarbodiimide (Aldrich) was used. The formed precipitate was separated by filtration and the yellow filtrate was washed with 2 mol L^{-1} hydrochloric acid and brine, dried ($MgSO_4$), and concentrated. Column chromatography on silica, followed by preparative thin layer chromatography (dichloromethane/ethyl acetate 2:1 and 4:1) gave **1a** (60 mg, 20%) as yellow solid, mp 136 °C (dec.). R_f (dichloromethane/ethyl acetate 2:1) = 0.78; R_f (dichloromethane/ethyl acetate 4:1) = 0.38. ESR (X-Band, THF): $g = 2.0037$, $a = 14.1$ G. FD-MS: $m/z = 350.7$ (100%, M^+). IR (KBr): $\tilde{\nu}$ [cm^{-1}] = 3330, 3032, 2958, 2926, 2854, 1662, 1622, 1520, 1502, 1464, 1434, 1400, 1358, 1316, 1286, 1246, 1180, 1160, 818.

Model compound ***2****: N-(4′-*Amino-biphenyl-4-yl)-2,2,5,5-tetramethyl-1-oxyl-2,5-dihydro-1*H*-pyrrol-3-carboxamide **1a** (23 mg, 66 mol) and 2-(4-isothiocyanatobenzyl)-1,4,7,10-tetraazacyclododecane-1,4,7,10-tetraacetic acid (p-SCN-Bn-DOTA, 36 mg, 66 mol, Macrocyclics, Dallas, TX) were dissolved in *N*,*N*-dimethylformamide (15 ml) and stirred overnight. The solvent was removed in vacuo to give crude **2** (59 mg) as golden-brownish solid, which was not further purified, mp 120–125 °C (dec.). ESR (X-band, THF/water): $g = 2.0035$, $a = 14.8$ G. IR (KBr): $\tilde{\nu}$ [cm^{-1}] = 3582, 3300, 3104, 3060, 3026, 2956, 2928, 2854, 2652, 2058, 1734, 1720, 1672, 1656, 1526, 1508, 1500, 1416, 1318, 1156, 1130, 824, 804. Attempts to separate **2** from p-SCN-Bn-DOTA and **1a** by preparative thin layer chromatography (*N*,*N*-dimethylformamide/dichloromethane 1:20 → 1:1) and the use of inverse phase chromatography failed, the crude product being of max 60% purity.

2.2. EPR measurements

All experiments were performed at X-band frequencies (9.3–9.4 GHz) with a Bruker Elexsys 580 spectrometer equipped with a Bruker Flexline split-ring resonator ER 4118X_MS3. Spectra were detected by field-swept echo-detected EPR and relaxation measurements were performed with an inversion-recovery sequence π–T–$\pi/2$–τ–π–τ–echo with the recovery delay starting at time $T_0 = 400$ ns, an inversion pulse length of 24 ns and observer pulses lengths of 52 and 104 ns for the $\pi/2$ and π pulse, respectively. The integration window for the echo matched the detection π pulse length of 104 ns. The $\pi/2$ pulse was phase cycled $[+(+x) - (-x)]$ to cancel receiver offsets and avoid any contributions from a free induction decay or two-pulse echoes involving the inversion pulse. Temperature was controlled using a cryostat ER-4118 CF and temperature controller ER4112-HV. After setting a new temperature the system was allowed to equilibrate for at least 20 min.

2.3. Monte Carlo simulations

All computations were performed within the Matlab (The MathWorks, Natick, MA) environment. In Monte Carlo simulations of homogeneous distributions either only the distance (test of Eqs. (13) and (14)) or the distance and angles θ_g between the magnetic field and the unique axis of the Dy^{3+} g tensor and θ between the magnetic field and the spin–spin vector were varied. Uniformly distributed random numbers ρ_i were generated and the distance was computed as $r = R\rho_1^{1/3}$, where R is the radius of the simulation sphere. This corresponds to a scaling of the number of centers with distance as r^2, which in turn corresponds to a homogeneous spatial distribution. The angles were computed by $\cos\theta_g = \rho_2$ and $\cos\theta = \rho_3$. Since $\sin\theta d\theta = d\cos\theta$, this ensures that all trials contribute with the same weight. For each trial, the relaxation rate for dipole–dipole relaxation was computed and an exponential decay with this rate added to the simulated signal. At the end the signal was normalized to the number of trials and fitted by a stretched exponential with exponent 1/2 or by a biexponential decay. From the fits the time τ_1, where the signal had decayed to $1/e$, was determined and an average relaxation rate $\bar{k} = 1/\tau_1$ was computed. Convergence of $\bar{k}$ with respect to both R and the number of Monte Carlo trials was tested. We find that $R = 50$ nm is sufficient to compute relaxivities with an error of less than 0.1%. Tests of Eqs. (13) and (14) were performed with up to 2 million trials, while computations with 200,000 trials were used in simulations of concentration dependence. Test simulations were performed with and without exclusion of a sphere with radius of 1 nm around the slowly relaxing center. No significant influence of this exclusion sphere on the results was observed for concentrations up to 10 mM. All simulations were performed for a field of 330 mT corresponding to X-band frequencies unless stated otherwise.

2.4. Molecular modeling

The conformer distribution of model compound **2** was estimated by a Monte Carlo conformer search with the software package Titan (Wavefunction Inc., Irvine, CA) using the MMFF94 force field and Gd^{3+} as a lanthanide ion. The N—O group of the nitroxide was substituted by a keto group to avoid difficulties with force field parametrization. From the 100 lowest energy conformers the 8 *Z,Za* conformers were selected and the mean distance between the lanthanide ion and the midpoint of the C=O bond was computed.

3. Theory

3.1. Dipolar relaxation enhancement by dysprosium complexes

We consider dipole–dipole relaxation of a slowly relaxing spin by a fast relaxing spin in the limit of weak coupling. The relaxation enhancement is defined as the difference of the inverse relaxation times of the slowly relaxing spin in the presence and absence of the fast relaxing spin,

$$\Delta k = \frac{1}{T_{1s}} - \frac{1}{T_{1s,0}}. \tag{1}$$

By extension of the seminal treatment [37,38] to electron spins the following expression for Δk as a function of distance r between the two spins and angle θ between the spin–spin vector and the static field was derived [23]

$$\Delta k(r,\theta) = S(S+1)\frac{g_s^2 g_f^2 \mu_0^2 \mu_B^4}{(4\pi)^2 \hbar^2 r^6}[f_B + f_{CD} + f_{EF}] \tag{2}$$

with

$$f_B = \frac{1}{6}(1-3\cos^2\theta)^2 \frac{T_{2f}}{1+(\omega_f-\omega_s)^2 T_{2f}^2},$$
$$f_{CD} = 3\sin^2\theta\cos^2\theta \frac{T_{1f}}{1+\omega_s^2 T_{1f}^2},$$
$$f_{EF} = \frac{3}{2}\sin^4\theta \frac{T_{2f}}{1+(\omega_f+\omega_s)^2 T_{2f}^2}, \tag{3}$$

where μ_0 is the permittivity of vacuum, μ_B the Bohr magneton, and S, g_f, T_{1f} and $T_{2\,f}$ are the spin quantum number, g value, longitudinal and transverse relaxation time of the fast relaxing spin, respectively. The angle between the spin–spin vector and the static magnetic field is θ. As the zero-field splitting lifts ground state degeneracy we assume that only the levels of a Kramers doublet are significantly populated, so that Dy^{3+} can be treated as an effective spin $S = 1/2$ [39]. Hence g_f is to be interpreted as an effective g value. As each of the eight Kramers doublets in the $^6H_{15/2}$ ground term can be described by an effective spin $S = 1/2$, population of higher-lying Kramers doublets would only lead to a tolerable distance error similar to the one estimated below for uncertainties in the effective g values. With these parameters, the magnetic field B_0 and the g_s value of the slowly relaxing spin, the resonance frequencies of the two spins in angular frequency units are given by

$$\omega_s = g_s \mu_B B_0/\hbar, \tag{4}$$

and

$$\omega_f = g_f \mu_B B_0/\hbar. \tag{5}$$

Unlike in the original formula, as given in Ref. [32], we assume pure dipole–dipole relaxation without a contribution by exchange coupling between the two spins. This is appropriate at distances of 1.5 nm or longer [42]. The coefficients f_B, f_{CD}, and f_{EF} are related to the B-, C, D- and E, F-terms of the dipole–dipole alphabet, respectively.

The g_f value, which enters both into the amplitude of the dipole–dipole coupling and into frequency ω_f, is strongly anisotropic for lanthanides. To a good approximation, the g matrix has axial symmetry with principal values $g_{\parallel f}$ and $g_{\perp f}$, so that we have

$$g_f = (g_{\perp f}^2 \sin^2\theta_g + g_{\parallel f}^2 \cos^2\theta_g)^{1/2}, \tag{6}$$

where θ_g is the angle between the static field and the unique axis of the lanthanide g tensor. Such g anisotropy leads to an orientation-dependent deviation of the quantization axis of the lanthanide spin from the magnetic field direction so that Eq. (3) is no longer strictly valid [40,41]. In the present contribution we neglect the minor effect on the dipole–dipole coupling that arises from this tilt of the quantization axis while we include the major effect of the orientation dependence of g_f. In the following, this is referred to as Likhtenshtein approximation [24].

Furthermore we assume that at temperatures of 20 K and above lanthanide ions are in a fast relaxation limit, so that $T_{1f} = T_{2\,f}$, and that orientation dependence of T_{1f} is negligible. With these assumptions Δk depends on T_{1f}, the two angles θ and θ_g, the g values of both spins, and on distance r. For given parameters T_{1f}, θ and θ_g we have

$$\Delta k = C(T_{1f},\theta,\theta_g)/r^6, \tag{7}$$

where C is an orientation-dependent relaxivity.

An orientation-averaged relaxivity $\bar{C}$ is required to analyze measurements on powders or frozen solutions. Such orientation averaging introduces a complication, as the sum of exponential decays with different rate constants $\Delta k(r,\theta,\theta_g)$ is not an exponential decay. We thus need a new single relaxation parameter that characterizes the non-exponential decay curves. The most natural choice is

$$\overline{\Delta k} = 1/\tau_1, \tag{8}$$

where τ_1 is the time where the signal has decayed to $1/e$ of its value at $t = 0$.

Implicitly τ_1 is defined by

$$1/e = \int w(\Omega)\exp[-\Delta k(\Omega)\tau_1]\mathrm{d}\Omega = \int w(\Omega)\exp\left[-C(\Omega)\tau_1/r^6\right]\mathrm{d}\Omega, \tag{9}$$

where the integration variable Ω characterizes orientation (θ_g,θ) and $w(\Omega)$ is a normalized weighting factor ($\int w(\Omega)\mathrm{d}\Omega = 1$). In Eq. (9) $C(\Omega)$ depends on orientation but not on distance, while τ_1 depends on distance but not on orientation. Both quantities depend on T_{1f}. Suppose now that τ_1 is known at certain distance r_1. If $\tau_1(r) < (r/r_1)^6\tau_1(r_1)$ the integrand at distance r would be larger than at distance r_1 for all Ω, so that the left-hand side of Eq. (9) would be larger than $1/e$, which contradicts the definition of τ_1. If $\tau_1(r) > (r/r_1)^6\tau_1(r_1)$ the integrand at distance r would be smaller than at distance r_1 for all Ω, so that the left-hand side of Eq. (9) would be smaller than $1/e$, which also contradicts the definition. Hence τ_1 at any other distance r must be given by $\tau_1(r) = (r/r_1)^6\tau_1(r_1)$ and $\overline{\Delta k}$ can be written as

$$\overline{\Delta k} = \frac{1}{\tau_1} = \frac{\overline{C}}{r^6} \tag{10}$$

with an average relaxivity $\overline{C}$ that depends on T_{1f} but not on orientation and distance.

This average relaxivity can be determined for any given value T_{1f} by computing the orientation-averaged decay

$$V(t) = \frac{\int\int \exp[-\Delta k(r,\theta,\theta_g)t]\sin\theta\,\mathrm{d}\theta\sin\theta_g\,\mathrm{d}\theta_g}{\int\int \sin\theta\,\mathrm{d}\theta\sin\theta_g\,\mathrm{d}\theta_g} \tag{11}$$

for an arbitrary value of r, determining the $1/e$-time τ_1 of this decay, and solving Eq. (10) for $\overline{C}$. Independent integration over the two angles is based on the assumption that the orientations of the spin–spin vector, the unique axis of the lanthanide g tensor, and the static field B_0 are uncorrelated with each other.

We have performed numerical simulations assuming an axial g tensor with $g_{\perp f} = 14$ and $g_{\parallel f} = 4.2$ as suggested by the spectrum of the EDTA complex of Dy^{3+} given by Blum et al. [43] and an isotropic g value $g_s = 2.0059$ for the nitroxide. We have also varied the principal g values within a reasonable range for Dy^{3+} ($g_{\perp f} = 0 \ldots 18$, $g_{\parallel f} = 18 \ldots 0$) and find that $\overline{C}$ changes by less than 40%, corresponding to an uncertainty of distances of less than 7%.

Based on these simulations we have tested whether decay curves $V(t)$ defined by Eq. (11) can be fitted by simple smooth decays (Fig. 2a). While exponential fits of the form $A\exp(-t/T_1)$ with two adjustable parameters A and T_1 perform poorly, stretched exponential fits of the form $A\exp\left[-(t/T_1)^x\right]$ with three adjustable parameters A, T_1, and x are somewhat better and biexponential fits of the form $A_1\exp(-t/T_{1,1}) + A_2\exp(-t/T_{1,2})$ with four adjustable parameters A_1, A_2, $T_{1,1}$ and $T_{1,2}$ provide good estimates of τ_1. Such fits are useful for analyzing noisy experimental decay curves, as τ_1 can be determined with higher precision from the smooth noise-averaged curve than directly from the experimental data. Note that the individual parameters A_1, A_2, $T_{1,1}$ and $T_{1,2}$ of the biexponential decay do not have any physical meaning.

Numerical computations were performed for 17 equally spaced distances in the range between 2 and 10 nm for different values of T_{1f} and the dependence of $\overline{\Delta k}$ on r was fitted by Eq. (10). A typical result is shown in Fig. 2b. We find that our numerical results are in good agreement with Eq. (10). Using an average relaxivity $\overline{C}$ for distance measurements between a nitroxide and a lanthanide ion is thus justified.

We have also tested the dependence of $\overline{C}$ on T_{1f}. For dysprosium–nitroxide pairs our numerical computations reveal a single maximum of the average relaxivity $\overline{C}$ at $T_{1f} = 1.2 \times 10^{-11}$s. This value is attained at the temperature of maximum relaxation enhancement, which can be determined experimentally. Distance measurements at this temperature do not require any further calibration as all parameters are known and $\overline{C}$ can thus be computed numerically. However, precision may be limited by the quality of the g value estimates for the lanthanide and by deviations from the Likhtenshtein approximation.

Since T_{1f} is expected to vary monotonically with temperature, this parameter can be determined indirectly in a broader temperature range from measurements of the temperature dependence of relaxation enhancement. For that we assume an empirical power law with two parameters

$$T_{1f}/s = 1.2 \times 10^{-11}\left(\frac{T_{\max}}{T}\right)^p, \tag{12}$$

where $T_{\max}$ is the temperature at which maximum relaxivity is experimentally observed and p is a scaling exponent that is determined by fitting the experimentally observed temperature depen-

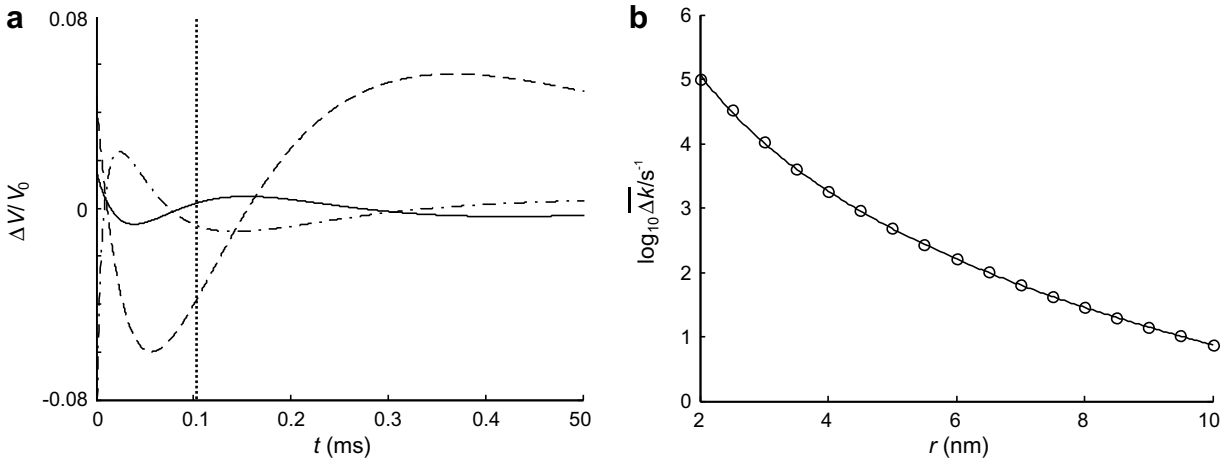

Fig. 2. Simulations for validation of an orientation-averaged relaxivity. Parameters: $r = 5$ nm, $T_{1f} = 1.3 \times 10^{-11}$ s, $B_0 = 0.33$ T. (a) Residuals of best fits of an orientation-averaged signal decay by an exponential decay (dashed line), stretched exponential (dash-dot line) and biexponential decay (solid line). The vertical dotted line designates time τ_1 when the signal has decayed to $1/e$ of its value at $t = 0$. (b) Dependence of the orientation-averaged relaxation rate enhancements $\overline{\Delta k}$ on distance. Open circles are numerically simulated values while the solid line is a fit according to Eq. (10).

dence of $\overline{\Delta k}$. From the known temperature dependence of T_{1f} we can then determine $\overline{C}(T)$ using Eqs. (2)–(6), (11) and (10). With $\overline{C}$ in turn the distance between the two spins can be determined. This approach does not require calibration of the technique with a model substance, as the temperature dependence can be measured on the very sample whose distance is to be determined. Furthermore the approach does not require a direct measurement of T_{1f} but relies on the assumption $T_{1f} = T_{2f}$.

3.2. Relaxation enhancement by a uniform distribution of fast relaxing centers

Alternatively the technique can be calibrated by measuring relaxation enhancement in homogeneous mixed solutions of a nitroxide spin probe and a lanthanide complex. This approach relies on the known concentration dependence of relaxivity as it was derived for the analogous case of paramagnetic relaxation of nuclear spins [44–46]. The original theoretical treatment allows for diffusion of the slowly relaxing spins, which may be either translational diffusion or spin diffusion. In solid matrices below 80 K translational diffusion is negligible. Spin diffusion of nitroxides is also expected to be negligible on the time scale of the relaxation measurements, if label concentrations of 250 μM or less are used, as is common in SDSL experiments on proteins.

In the limit of negligible diffusion, the normalized decay is described by

$$V(t)/V(0) = \exp(-(t/\tau_1)^{1/2}) \tag{13}$$

with

$$\tau_1^{-1} = \frac{16\pi^3}{9}\overline{C}(N_A c_{Ln})^2, \tag{14}$$

where N_A is Avogadro's constant and c_{Ln} is the concentration of the lanthanide complex. The numerical prefactor depends on an estimate for a critical radius and different authors have given different values [44–46].

In particular, the value in [46] was derived with the assumption that $\omega_0 T_{1f} \gg 1$, where in our context ω_0 could be any of ω_s, $\omega_f - \omega_s$, or $\omega_f + \omega_s$. However closer inspection reveals that the scaling behavior and numerical prefactor cannot depend on correlation time as long as the spatial positions of the fast relaxing spins are fixed and spin diffusion of these spins can be neglected on the time scale of the experiment.

The prefactor used in Eq. (14) was found to be within 0.2% of the value determined by numerical Monte Carlo simulations. We attribute this slight deviation to numerical imprecision in adding decay functions over a very broad range of rate constants. In any case, such a small deviation is not significant for application as it corresponds to a relative error of less than 3.3×10^{-4} for the distance. The simulations also confirm the stretched exponential decay with exponent 1/2 described by Eq. (13) and the scaling of τ_1^{-1} with the square of the concentration (data not shown).

Eq. (14) was derived for a situation where each pair (r,θ) corresponds to a single value of the dipole–dipole relaxation rate. Due to the dependence on θ_g each pair (r,θ) corresponds to a distribution of relaxation rates. Since the average relaxation rate scales with r^{-6} we may expect that the scaling with c_{Ln}^2 is also maintained. This is indeed confirmed by simulations for the concentration range between 0.5 and 10 mM. However, the distribution of rates leads to a decay curve that does not conform to Eq. (13). Again, this curve can be fitted nicely by a biexponential decay and an average relaxation rate can be defined by Eq. (8). This average relaxation rate scales with c_{Ln}^2 (Fig. 3). The fit provides a value for the average relaxivity $\overline{C}$ that is similar to the value obtained from analyzing distance dependence, but does not agree exactly. We attribute this to different effects on the 1/*e*-time τ_1 when averaging exponential and stretched exponential decays. A quantitative comparison is made in Section 4 below.

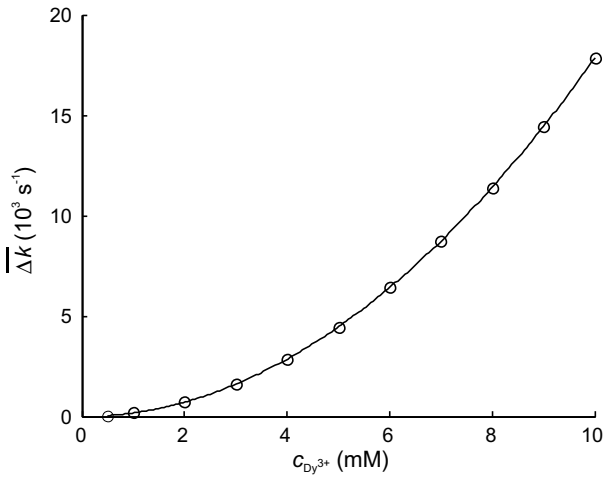

Fig. 3. Scaling of the average relaxation enhancement $\overline{\Delta k}$ in homogeneous solution with concentration $c_{Dy^{3+}}$ of a Dy^{3+} complex. Open circles are results of Monte Carlo simulations with $T_{1f} = 1.3 \times 10^{-11}$ s, $B_0 = 0.33$ T and $\overline{\Delta k}$ determined as the inverse 1/*e*-time of the fit of a biexponential decay function to the data. The solid line is a fit of a square law $\overline{\Delta k} = A c_{Dy^{3+}}^2$ to the simulated data.

Thus the average relaxivity $\overline{C}$ can also be determined from a measurement of the relaxation enhancement of nitroxide spins at a known concentration of a lanthanide complex. Such calibration does not require any knowledge on relaxation times or principal values of the *g* tensor of the lanthanide ion and is not based on the assumption $T_{1f} = T_{2f}$. Eq. (14) can also be used to correct for intermolecular effects if the concentration of lanthanide labels is known and a homogeneous distribution in space can be assumed for the system of interest.

Note that dipolar line broadening for an A spin due to a homogeneous distribution of B spins that do not relax on the time scale of the observation also leads to a Lorentzian lineshape, corresponding to an enhancement of the transversal relaxation time T_2 that is proportional to concentration, not to its square [47].

4. Results

4.1. Relaxation of nitroxide spin probes in the absence of paramagnetic lanthanide ions

In EPR spectroscopy relaxation data are usually derived from saturation recovery experiments. Such experiments have the advantage that they are less susceptible to contributions of spectral diffusion than inversion recovery experiments but they are also less sensitive. This applies particularly to echo detection, which we prefer to probe-field detection, as the former detection technique is much less susceptible to instabilities of the resonator frequency and thermal artifacts. In echo-detected inversion recovery experiments the multiplex advantage of probe-field detection can be compensated by applying pulses with a much larger excitation bandwidth than the probe field and thus detecting a much larger fraction of spins. True saturation over such a broad frequency band is harder to achieve. Therefore, we have to consider the question whether contributions from spectral diffusion affect precision and range of relaxation-based distance measurements.

Spectral diffusion contributes in the same way to $T_{1s,0}$ and T_{1s}. Hence, this contribution cancels in the difference Δk that is used to estimate the distance. For measurements of long distances, a spectral diffusion contribution would still be detrimental, as it

leads to a shorter apparent $T_{1s,0}$. Very small relaxation enhancements would then be more difficult to detect. Therefore, we have compared our data on relaxation of TEMPOL in a 60% glycerol:40% water (v/v) mixture obtained by echo-detected inversion recovery measurements to published values for the 4-oxo spin label TEMPONE in a 1:1 (v/v) mixture of glycerol and water obtained with probe-field detected saturation recovery measurements. At temperatures of 40, 60, and 80 K our data superimpose almost perfectly with published plots for TEMPONE in a slightly different matrix [48] (data not shown). By applying a short inversion pulse followed by a detection echo with about four times smaller bandwidth we can thus suppress any contribution from spectral diffusion at these temperatures. At a temperature of 20 K, our relaxation time is by about a factor of 1.8 shorter than the one derived from the published plot. This may be due to the slight differences in the spin label and matrix or due to a contribution by spectral diffusion that becomes significant at the very long $T_{1s,0}$ encountered at a temperature as low as 20 K. A more precise comparison of saturation recovery and inversion recovery may thus be required for measurements that approach the long distance limit at such low temperatures. This is, however, beyond the scope of the present work.

Throughout the whole temperature range from 20 to 80 K our own relaxation data for TEMPOL in the absence of a paramagnetic lanthanide complex can be fitted by an empirical power law

$$T_{1s,0}/\mathrm{s} = 193(T/\mathrm{K})^{-3}. \quad (15)$$

4.2. Temperature dependence of dysprosium-induced relaxation

The temperature dependence of relaxation enhancement of TEMPOL (250 μM) by 10 mM of the Dy^{3+}-DOTA complex in a glassy glycerol–water mixture with 60% (v/v) glycerol was measured between 20 and 60 K at temperature increments of 2 K. The data are presented in Fig. 4 together with a fit obtained by varying parameters T_{max} and p in Eq. (12). Within the range from 20 to 60 K the experimental data are fitted rather nicely by $T_{max} = (41.5 \pm 1)$ K and $p = 2.4 \pm 0.1$.

An additional measurement was performed at 80 K. This data point was not included in the fit, as a relaxation study of several systems has shown that in water:glycerol mixtures additional thermally activated relaxation processes contribute at temperatures around 80 K or higher [48].

Consideration of the individual terms in Eq. (3) shows that at low temperatures the C, D term (dotted line in Fig. 4) dominates as was already remarked upon earlier [26]. However, for precise measurements it is not advisable to neglect the B term (dashed line) and E, F term (dash-dot line).

With the parameters obtained from this fit, T_{1f} can be computed in the temperature range from 20 to 60 K and theoretical relaxivities $\overline{C}_{th,r}$ and $\overline{C}_{th,c}$ can be obtained by Monte Carlo simulations of the distance and concentration dependence of $\overline{\Delta k}$, respectively. These values are given in Table 1. The differences between the two sets of values are probably due to the different effects on τ_1 that arise in averaging of a distribution of exponential decays and stretched exponential decays. Values obtained from the concentration dependence are larger by a factor 1.18 ± 0.10. Owing to the r^{-6} dependence of relaxation enhancement, this difference corresponds to an error of less than 4% in distance measurements calibrated by the concentration dependence, even if no correction is made.

4.3. Concentration dependence of dysprosium-induced relaxation

Relaxation enhancement of TEMPOL by the Dy^{3+}-DOTA complex in homogeneous glassy frozen solution was experimentally studied in the concentration range from 0.2 to 10 mM at temperatures of 20, 40, and 60 K. No significant enhancement could be detected at 0.2 mM (data not shown). Data for the range from 1.25 to 10 mM are plotted in Fig. 5 together with best fits according to

Table 1
Average relaxivities of the Dy^{3+}-DOTA complex in a glassy 0.6:0.4 (v/v) mixture of glycerol and water at selected temperatures obtained by Monte Carlos simulations of the dependence of $\overline{\Delta k}$ on distance ($\overline{C}_{th,r}$) and on concentration ($\overline{C}_{th,c}$) and by measurements of the concentration dependence of $\overline{\Delta k}$ ($\overline{C}_{exp,c}$)

Temperature (K)	$\overline{C}_{th,r}$ (10^6 s^{-1} nm^6)	$\overline{C}_{th,c}$ (10^6 s^{-1} nm^6)	$\overline{C}_{exp,c}$ (10^6 s^{-1} nm^6)
20	3.04	3.89	4.12
40	7.48	10.11	13.0
60	6.39	6.88	9.01

Parameter T_{1f} was computed from Eq. (12) assuming $T_{max} = 41.5$ K and $p = 2.4$ (see text).

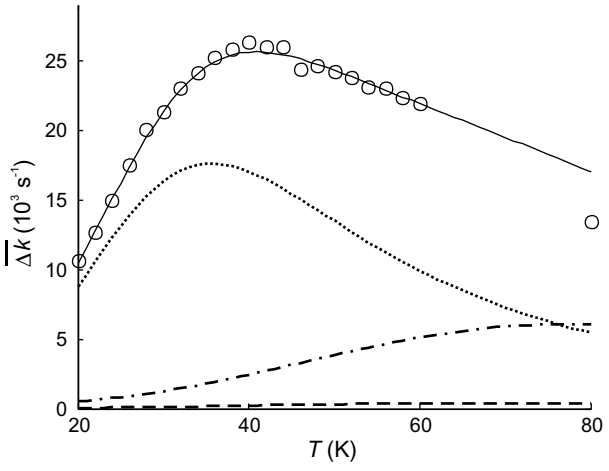

Fig. 4. Temperature dependence of the relaxation enhancement $\overline{\Delta k}$ of TEMPOL by 10 mM Dy^{3+} DOTA in a glassy 0.6:0.4 (v/v) mixture of glycerol and water. Open circles are experimental data with $\overline{\Delta k}$ determined as the inverse 1/e-time of the fit of a biexponential decay function to the data. The solid line is a fit based on an empirical power law for T_{1f} (Eq. (12) with $T_{max} = (41.5 \pm 1)$ K and $p = 2.4 \pm 0.1$). Individual contributions of the B term (dashed line), C, D term (dotted line), and E, F term (dash-dot line) of the dipole–dipole alphabet are also shown.

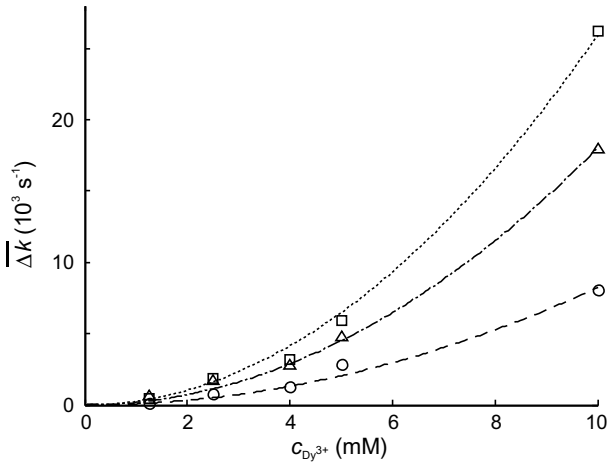

Fig. 5. Concentration dependence of the relaxation enhancement $\overline{\Delta k}$ of TEMPOL by Dy^{3+} DOTA in a glassy 0.6:0.4 (v/v) mixture of glycerol and water at temperatures of 20 K (open circles and dashed line), 40 K (squares and dotted line), and 60 K (triangles and dash-dot line). The lines are best fits by Eq. (14) assuming $\overline{\Delta k} = \tau_1^{-1}$.

Eq. (14). We assume $\tau_1^{-1} = \overline{\Delta k}$ and thus determine average relaxivities $\overline{C}_{\mathrm{exp},c}$, which are given in Table 1.

In comparing the experimental data with the results of Monte Carlo simulations thermal contraction of the glycerol/water glass has to be considered. This contraction leads to an increase of the concentration of the lanthanide complex compared to room temperature where the solutions were prepared. Unfortunately thermal expansion coefficients for glycerol/water mixtures down to such low temperatures appear to be unknown. Hence no correction can be made for this effect. Note that thermal expansion coefficients could be obtained from such EPR relaxation measurements in cases where the temperature dependence of T_{1f} and T_{2f} can be determined independently. Given the unknown thermal expansion coefficient, uncertainties in the g tensor of Dy^{3+} DOTA, and neglect of the tilt of the Dy^{3+} quantization axis in the Likhtenshtein approximation, agreement between relaxivity values obtained from temperature and concentration dependence can be considered as satisfying.

4.4. Distance measurement on a model compound

The experimentally determined relaxivities of the Dy^{3+}-DOTA complex in glycerol/water glass allow for deriving spin-to-spin distances from experimentally observed intramolecular relaxation enhancements by using Eq. (10). To test this approach measurements were performed for model compound **2**, using La^{3+} as a diamagnetic control to determine $T_{1s,0}$ and Dy^{3+} for relaxation enhancement. Determination of $\overline{\Delta k}$ by direct substraction of the relaxation rate of the diamagnetic complex from the one of the paramagnetic complex is only feasible if lanthanide labeling of the substance is complete. This requires a pure heterogeneously bilabeled sample. The same requirement exists for FRET measurements and is considered as a major obstacle for broad application of this technique [49]. Therefore, we have tested whether EPR distance measurements via relaxation enhancements are also feasible with partially labeled samples, if data are analyzed in a different way.

To that end we use the raw product of the synthesis of model compound **2**, which is a mixture of unlabeled molecules, singly nitroxide labeled molecules, singly DOTA-labeled molecules and the wanted bilabeled molecule. Rather than determining the concentration of DOTA ligands by titration we used an excess of the lanthanide trichloride. Despite all these imperfections in sample preparation the intramolecular contribution to the relaxation is clearly seen when comparing primary experimental data between the Dy^{3+} and La^{3+} complexes (Fig. 6a).

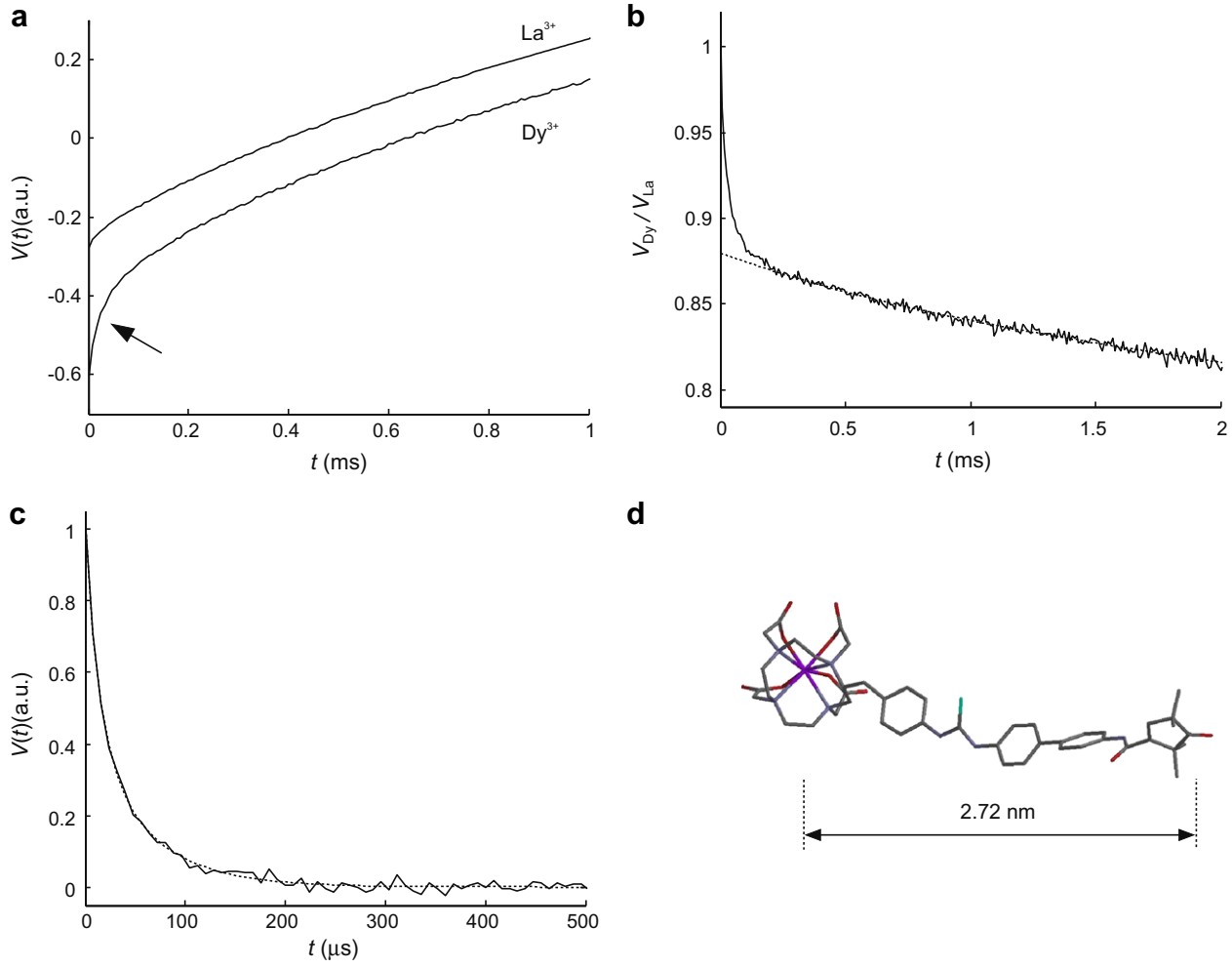

Fig. 6. Distance measurement on the raw product of the synthesis of model compound **2**. (a) Inversion recovery curves for the complexes with diamagnetic La^{3+} and paramagnetic Dy^{3+}. The arrow marks the intramolecular decay component. For better visibility, the Dy^{3+} curve is vertically shifted. (b) Result of the reference deconvolution (solid line) and fit of the intermolecular decay component by a biexponential decay function (dotted line). A concentration of 280 μM is found. (c) Normalized intramolecular decay component obtained by substracting the biexponential fit of the intermolecular component from the result of reference deconvolution (solid line). The dotted line is a fit by a biexponential decay function. A distance of 2.65 nm is found when using the experimentally determined relaxivity $\overline{C}_{\mathrm{exp},c}$. (d) Force-field optimized structure (MMFF94 force field) of one selected (*Z*,*Za*) conformation of the model compound. The mean distance predicted for eight different (*Z*,*Za*) conformations is 2.72 nm.

In this situation, relaxation contributions in the absence and presence of the paramagnetic lanthanide are best removed by reference deconvolution, i.e., by dividing the data set measured with Dy^{3+} by the one measured with La^{3+}. The result of such reference deconvolution (Fig. 6b) implies that about 12% of the nitroxide labels show the fast decay corresponding to intramolecular relaxation enhancement by Dy^{3+}, while the remaining 88% exhibit only intermolecular relaxation enhancement. The latter fraction was determined by extrapolating the fitted intermolecular decay curve to zero time.

The intermolecular contribution was fitted by a biexponential decay function at times $t > 0.25$ ms. The best fit, shown as a dotted line in (Fig. 6b), provides a $1/e$-time $\tau_1 = 50.4$ ms. Using the experimental relaxivity of $\overline{C}_{\mathrm{exp},c}$ this corresponds to a Dy^{3+} concentration of 280 μM in line with expectations. After substracting this contribution, the purely intramolecular contribution remains. The biexponential fit of this contribution provides a $1/e$-time $\tau_1 = 26.4$ μs. By again using the experimental relaxivity $\overline{C}_{\mathrm{exp},c}$ we obtain a distance of 2.65 nm. If we use $\overline{C}_{\mathrm{th},r}$ instead, we find a distance of 2.41 nm and with $\overline{C}_{\mathrm{th},c}$ a distance of 2.49 nm.

With a linker based on a thioether one might not have expected a well defined distance. Force-field computations in vacuum suggest that different (*Z*,*Z*), (*E*,*Z*), and (*E*,*E*) conformations at the thioether are all similar in energy. This would lead to a broad distribution of distances extending to well below 2 nm, which is in contradiction with our experimental results. However, high-resolution NMR studies of thioethers have demonstrated that in solution usually one of the conformers strongly dominates [50]. In hydroxylic solvents the (*Z*,*Za*) conformers are preferentially populated. We have computed 100 low-energy conformers in vacuum, using a Monte Carlo conformer search as implemented in the Titan software package with the MMFF94 force field. By selecting the (*Z*,*Za*) conformers we obtain a mean distance of 2.72 nm in rather good agreement with the experimental result.

In fact, the experimental finding of a slightly lower distance than expected could be due to the r^{-6} averaging that overemphasizes the contribution of conformations with short distances, as was recently pointed out in a study on copper(II)-induced relaxation of nitroxide spin labels [34]. However, considering that we computed the structural ensemble in vacuum and that solvation effects are important for thioethers, we refrain from claiming that the deviation is solely due to this effect. The larger deviation when using $\overline{C}_{\mathrm{th},r}$ is expected due to uncertainty in the lanthanide *g* values and use of the Likhtenshtein approximation in the numerical computations.

5. Discussion

5.1. Correlated temperature and frequency dependence of relaxation enhancement

Our theoretical and experimental results suggest that precise distance measurements between paramagnetic lanthanide ions and nitroxides are feasible with moderate effort for calibration of the technique. With respect to the current study precision with calibration by temperature dependence could be improved by measurement of the principal *g* values of the lanthanide and by considering the tilt of the lanthanide quantization axis. Precision with calibration by concentration dependence could be improved by an independent measurement of the thermal contraction of the matrix. For application to biomacromolecules distance range and sensitivity have to be optimized. At given relaxivity the lower limit of the distance range is determined by the ring-down time t_{ring} after an inversion or saturation pulse which sets a lower limit to the τ_1 that can be measured. Assuming $t_{\mathrm{ring}} = 80$ ns and $\tau_1 > 5t_{\mathrm{ring}}$, we can estimate that distances down to about 1.1 nm could be measured at a temperature of 20 K at X-band frequencies. In principle, smaller relaxivities could be obtained with lanthanide ions other than Dy^{3+}. However, we expect that at distances below about 1.2 nm errors due to neglect of exchange coupling become too large. Given the size of the two probes such short distances can be considered as near contact. Therefore, the lower distance limit can be achieved without further optimization of the approach.

The upper distance limit is determined by the relaxivity contrast distance *R* that we define as

$$R = (2T_{1s,0}\overline{C})^{1/6}. \tag{16}$$

This definition assumes that a 50% change in relaxation rate with respect to the rate in the absence of the paramagnetic lanthanide can still be quantified. Based on Eq. (15) and the fit of the temperature dependence of $\overline{C}$, the temperature dependence of *R* was computed for the Dy^{3+} complex of DOTA in glassy 0.6:0.4 (v/v) mixtures of glycerol and water (Fig. 7). We find that the relaxivity contrast distance increases monotonously with decreasing temperature. This is because prolongation of the longitudinal relaxation time of the nitroxide in the absence of Dy^{3+} overcompensates the decrease in relaxivity. However, we caution against extrapolating that behavior to temperatures below 20 K. When temperature is further lowered relaxation behavior of both the nitroxide and the lanthanide complex will eventually deviate from the empirical power laws that we use and T_{2f} will become shorter than T_{1f}.

An obvious way of extending the distance range towards longer distances is variation of the static magnetic field. It has been found that relaxation in the absence of nearby paramagnetic centers only weakly depends on field between S-band and W-band frequencies [51]. The field dependence of the relaxivity contrast distance is then expected to be governed by the field dependence of the spectral density terms in Eq. (3). Each individual term attains its maximum when $1/T_{1f}$ equals the characteristic frequency. The characteristic frequency in turn scales linearly with field. At lower fields the maxima are thus attained at longer T_{1f}. If T_{1f} only weakly depends on frequency they are attained at lower temperatures and thus also at longer $T_{1s,0}$. Furthermore, as the effect of each term is linear in T_{1f}, maximum relaxivity is also larger at lower fields. The upper distance limit is thus expected to increase significantly when going to lower fields. We predict that relaxation-based distance measurements can surpass the distance range of pulsed EPR distance measurements based on direct determination of the di-

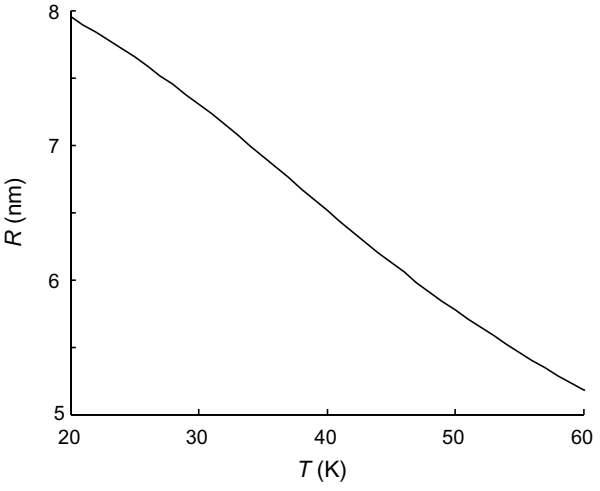

Fig. 7. Dependence of relaxivity contrast distance *R* on temperature for a Dy^{3+} DOTA relaxant in 0.6:0.4 (v/v) glycerol:water.

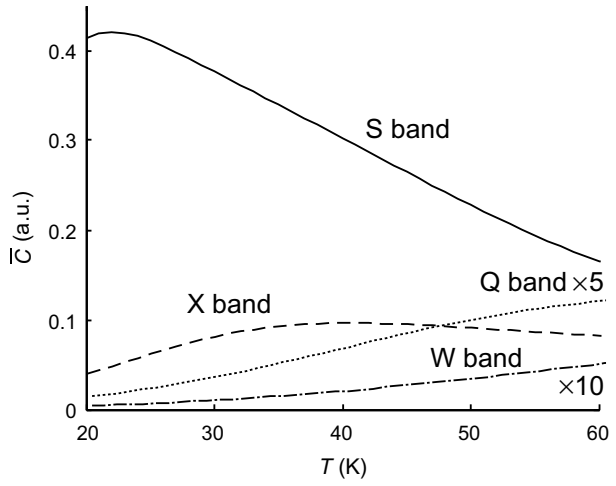

Fig. 8. Magnetic field and temperature dependence of relaxivity expected if the field dependence of the relaxation times of the nitroxide and the Dy^{3+}-DOTA complex in the absence of dipole–dipole interaction is weak. Simulations were performed with $T_{1f} = 1.2 \times 10^{-11}(41.5\ K/T)^{2.4}$ at fields of 75 mT (solid line, S-band), 330 mT (dotted line, X-band), 1.25 T (dashed line, magnified by a factor of 5, Q-band), and 3.35 T (dash-dot line, magnified by a factor of 10, W-band).

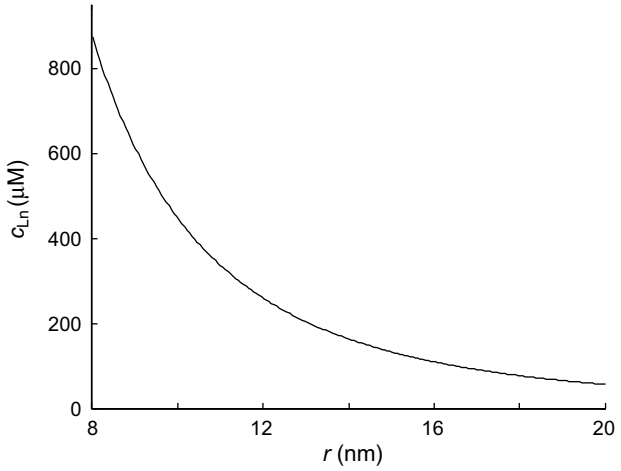

Fig. 9. Maximum permissible lanthanide concentration as a function of distance according to Eq. (17).

pole–dipole coupling. The effect of changes in static field on temperature dependence of relaxivity is illustrated in Fig. 8. For simplicity we have assumed that the field dependence of T_{1f} and $T_{1s,0}$ is insignificant.

5.2. Maximum lanthanide concentration

The measurement of long distances imposes an upper limit on lanthanide concentration as intermolecular decay components should be either negligible or at least distinguishable from intramolecular decay components. If we require that the intramolecular decay component exceeds the intermolecular one by a factor of four, this limit can be estimated from Eqs. (10) and (14) as

$$c_{Ln} = \frac{3}{2\pi^{3/2} r^3 N_A}. \tag{17}$$

This dependence is plotted in Fig. 9. Even at a distance of 20 nm a concentration of 50 μM would still be permissible. As inversion recovery curves can be measured down to concentrations of at least 5 μM with sufficient signal-to-noise ratio, the concentration limit does not seem to impose a serious restriction on extending distance range.

5.3. Sensitivity issues

The considerations on optimum measurement parameters suggest that the distance limit can be extended by going to lower temperatures and lower fields. In both cases sensitivity decreases, which suggests to perform the measurements at fields and temperatures that are adapted to the expected distances. The dependence of sensitivity on temperature can be estimated from the empirical power law for $T_{1s,0}$ and the temperature dependence of the Boltzmann factor. Signal-to-noise ratio can be improved by signal averaging and is proportional to the square root of the number of signal accumulations. The number of accumulations for a given measurement time scales as $1/T_{1s,0}$, as the permissible repetition rate scales like this. In the high-temperature limit the signal amplitude is proportional to $1/T$. For a power law $T_{1s,0} \propto T^{-p}$ the signal-to-noise ratio thus scales as

$$\left(\frac{S}{N}\right) \propto T^{p/2-1}. \tag{18}$$

For the power law with $p = 3$ that we found for nitroxides at X-band, the signal-to-noise ratio is thus proportional to the square root of temperature. Measurements at 60 K are then by a factor of about 1.73 more sensitive than those ones at 20 K.

6. Conclusion

Reexamination of the relaxation-enhancing properties of Dy^{3+} complexes on nitroxides demonstrates that relaxation-based distance measurements between lanthanide and nitroxide labels can provide data with a precision that is sufficient for structural modeling. Such measurements can be expected to be more sensitive than direct measurements of the dipole–dipole coupling and may give access to both shorter and longer distances than direct measurements. Disadvantages are the larger size of lanthanide labels, the necessity of calibration, and the requirement for attaching two different labels.

Two new approaches for calibration have been introduced that do not require model compounds with well defined distances. In the first approach, only the sample of interest is required. By measuring the temperature dependence of relaxation enhancement, the unknown relaxation parameters of the lanthanide ion and its relaxivity can be estimated. In the second approach homogeneous solutions of the nitroxide and the lanthanide complex are used. Both approaches have been found to provide similar results. The second approach requires fewer assumptions and may thus be more precise. Based on such calibration a distance of approximately 2.7 nm was measured in a model compound with incomplete lanthanide labeling and was found to be in satisfying agreement with expectations. Measurements of significantly longer distances appear feasible, in particular at lower fields and temperatures.

Routine use of this approach will require knowledge of the dependence of relaxivity on the environment of the lanthanide complex. Furthermore, the precision of the technique should be tested for a broad distance range by measurements on model compounds with well defined distances, and the temperature and field dependence of relaxivity should be studied in detail. Work along those lines is now in progress.

Acknowledgments

The authors thank Michelle Drechsler for help with the synthesis of model compound **2** and Dr. Dariush Hinderberger for EPR spectroscopic characterization of this model compound. Financial

support by Deutsche Forschungsgemeinschaft is gratefully acknowledged.

References

[1] A.D. Milov, K.M. Salikhov, M.D. Shirov, Application of ELDOR in electron-spin echo for paramagnetic center space distribution in solids, Fiz. Tverd. Tela (Leningrad) 23 (1981) 957–982.

[2] A.D. Milov, A.B. Ponomarev, Yu. D. Tsvetkov, Electron electron double-resonance in electron-spin echo-model biradical systems and the sensitized photolysis of decalin, Chem. Phys. Lett. 110 (1984) 67–72.

[3] S. Saxena, J.H. Freed, Double quantum two-dimensional Fourier transform electron spin resonance: distance measurements, Chem. Phys. Lett. 251 (1996) 102–110.

[4] P.P. Borbat, J.H. Freed, Multiple-quantum ESR and distance measurements, Chem. Phys. Lett. 313 (1999) 145–154.

[5] M. Pannier, S. Veit, A. Godt, G. Jeschke, H.W. Spiess, Dead-time free measurement of dipole–dipole interactions between electron spins, J. Magn. Reson. 142 (2000) 331–340.

[6] P.G. Fajer, Site directed spin labelling and pulsed dipolar electron paramagnetic resonance (double electron–electron resonance) of force activation in muscle, J. Phys. Condens. Matter 17 (2005) S1459–S1469.

[7] G. Jeschke, Ye. Polyhach, Distance measurements on spin-labelled biomacromolecules by pulsed electron paramagnetic resonance, Phys. Chem. Chem. Phys. 9 (2007) 1895–1910.

[8] O. Schiemann, T.F. Prisner, Long-range distance determinations in biomacromolecules by EPR spectroscopy, Q. Rev. Biophys. 40 (2007) 1–53.

[9] P.P. Borbat, J.H. Freed, Measuring distances by pulsed dipolar ESR spectroscopy: spin-labeled histidine kinases, Methods Enzymol. 423 (2007) 53–116.

[10] J. Bhatnagar, J.H. Freed, B.R. Crane, Rigid body refinement of protein complexes with long-range distance restraints from pulsed dipolar ESR, Methods Enzymol. 423 (2007) 117–133.

[11] G. Jeschke, A. Bender, H. Paulsen, H. Zimmermann, A. Godt, Sensitivity enhancement in pulse EPR distance measurements, J. Magn. Reson. 169 (2004) 1–12.

[12] P.P. Borbat, J.H. Davis, S.E. Butcher, J.H. Freed, Measurement of large distances in biomolecules using double-quantum filtered refocused electron spin–echoes, J. Am. Chem. Soc. 126 (2004) 7746–7747.

[13] J.E. Banham, C.R. Timmel, R.J.M. Abbott, S.M. Lea, G. Jeschke, A new tool for characterization of weak protein–protein interactions: evidence from DEER for the trimerization of a von Willebrand Factor A Domain in solution, Angew. Chem. Int. Ed. 45 (2006) 1058–1061.

[14] G. Jeschke, H. Zimmermann, A. Godt, How flexible are oligo(para-phenyleneethynylene)s?, Angew Chem. Int. Ed. 45 (2006) 7560–7564.

[15] W.L. Hubbell, C. Altenbach, Investigation of structure and dynamics in membrane proteins using site-directed spin-labeling, Curr. Opin. Struct. Biol. 4 (1994) 566–573.

[16] W.L. Hubbell, D.S. Cafiso, C. Altenbach, Identifying conformational changes with site-directed spin labeling, Nat. Struct. Biol. 7 (2000) 735–739.

[17] A.G. Maryasov, Y.D. Tsvetkov, Formation of the pulsed electron–electron double resonance signal in the case of a finite amplitude of microwave fields, Appl. Magn. Reson. 18 (2000) 583–605.

[18] L.J. Berliner, S.S. Eaton, G.R. Eaton (Eds.), Distance Measurements in Biological Systems by EPR, Biological Magnetic Resonance, vol. 19, Plenum, New York, 2000.

[19] J.E. Banham, C.M. Baker, S. Ceola, I.J. Day, G.H. Grant, E.J.J. Groenen, C.T. Rodgers, G. Jeschke, C.R. Timmel, Distance measurements in the borderline region of applicability of CW EPR and DEER: a model study on a homologous series of spin-labelled peptides, J. Magn. Reson. doi:10.1016/j.jmr.2007.11.023.

[20] J. Voss, J.H. Wu, W.L. Hubbell, V. Jacques, C.F. Meares, H.R. Kaback, Helix packing in the lactose permease of *Escherichia coli: distances between site-directed nitroxides and a lanthanide, Biochemistry 40 (2001) 3184–3188.*

[21] M.D. Vlasie, C. Comuzzi, A.M.C.H. van den Nieuwendijk, M. Prudencio, M. Overhand, M. Ubbink, Long-range-distance NMR effects in a protein labeled with a lanthanide–DOTA chelate, Chem. Eur. J. 13 (2007) 1715–1723.

[22] A.V. Kulikov, G.I. Likhtenshtein, Application of saturation curves for evaluating distances in biological objects by the method of double spin labels, Biofisika 19 (1974) 420–424.

[23] A.I. Kulikov, G.I. Likhtenshtein, The use of spin-relaxation phenomena in the investigation of the structure of model and biological systems by method of spin labels, Adv. Mol. Relax. Interact. Proc. 10 (1977) 47–78.

[24] G.I. Likhtenshtein, Depth of immersion of paramagnetic centers in biological systems, in: L.J. Berliner, S.S. Eaton, G.R. Eaton (Eds.), Biological Magnetic Resonance, vol. 19, Kluwer, New York, 2000, pp. 309–345.

[25] T. Sarna, J.S. Hyde, H.M. Swartz, Ion-exchange in melanin—electron-spin resonance study with lanthanide probes, Science 192 (1976) 1132–1134.

[26] J.S. Hyde, K.V.S. Rao, Dipolar-induced electron spin-lattice relaxation in unordered solids, J. Magn. Reson. 29 (1978) 509–516.

[27] W.E. Antholine, J.S. Hyde, H.M. Swartz, Use of Dy^{3+} as a free-radical relaxing agent in biological tissues, J. Magn. Reson. 29 (1978) 517–522.

[28] G.W. Brudvig, D.F. Blair, S.I. Chan, Electron spin relaxation of CuA and cytochrome a in cytochrome c oxidase. Comparison to heme, copper, and sulfur radical complexes, J. Biol. Chem. 259 (1984) 11001–11009.

[29] S.S. Eaton, G.R. Eaton, Interaction of Spin Labels with Transition Metals. Part 2, Coord. Chem. Rev. 83 (1988) 29–72.

[30] Y. Degliannakis, A.W. Rutherford, Spin-lattice relaxation of the Pheophytin, $Pheo^{-}$, radical of photosystem II, Biochemistry 35 (1996) 11239–11246.

[31] C.S. Klug, S.S. Eaton, G.R. Eaton, J.B. Feix, Ligand-induced conformational change in the ferric enterobactin receptor FepA as studied by site-directed spin labeling and time-domain ESR, Biochemistry 37 (1998) 9016–9023.

[32] S.S. Eaton, G.R. Eaton, Determination of distances based on T_1 and T_m effects, in: L.J. Berliner, S.S. Eaton, G.R. Eaton (Eds.), Biological Magnetic Resonance, vol. 19, Kluwer, New York, 2000, pp. 348–381.

[33] S. Lyubenova, M.K. Siddiqui, M.J.M. Penning de Vries, B. Ludwig, T.F. Prisner, Protein–protein interactions studied by EPR relaxation measurements: cytochrome c and cytochrome c oxidase, J. Phys. Chem. B 111 (2007) 3839–3846.

[34] S. Jun, J.S. Becker, M. Yonkunas, R. Coalson, S. Saxena, Unfolding of alanine-based peptides using electron spin resonance distance measurements, Biochemistry 45 (2006) 11666–11673.

[35] F. Arnesano, L. Banci, M. Piccioli, NMR structures of paramagnetic metalloproteins, Q. Rev. Biophys. 38 (2005) 167–219.

[36] J.-C.G. Bünzli, Luminescent lanthanide probes as diagnostic and therapeutic tools, in: A. Sigel, H. Sigel (Eds.), Metal Ions in Biological Systems, vol. 42, Marcel Dekker Inc., New York, 2004. (Chapter 2).

[37] N. Bloembergen, E.M. Purcell, R.V. Pound, Relaxation effects in nuclear magnetic resonance absorption, Phys. Rev. 73 (1948) 679–712.

[38] N. Bloembergen, On the interaction of nuclear spins in a crystalline lattice, Physica 15 (1949) 386–426.

[39] J.M. Hastings, L.M. Corliss, C.G. Windsor, Antiferromagnetic structure of dysprosium aluminum garnet, Phys. Rev. 138 (1965) A176–A177.

[40] Y. Degliannakis, Electron paramagnetic relaxation enhancement produced on T_1 by anisotropic g-tensors in rigid systems, Mol. Phys. 105 (2005) 2095–2108.

[41] The expressions from Ref. [40] cannot be applied as they are not invariant under permutation of the eigenvalues of the *g* tensor and corresponding changes in the Euler angles.

[42] G. Jeschke, Determination of the nanostructure of polymer materials by electron paramagnetic resonance spectroscopy, Macromol. Rapid. Commun. 23 (2002) 227–246.

[43] H. Blum, M.A. Cusanovich, W.V. Sweeney, T. Ohnishi, Magnetic interaction between dysprosium complexes and two soluble iron–sulfur proteins, J. Biol. Chem. 256 (1981) 2199–2206.

[44] D. Tse, S.R. Hartmann, Nuclear spin-lattice relaxation via paramagnetic centers without spin diffusion, Phys. Rev. Lett. 21 (1968) 511–514.

[45] I.J. Lowe, D. Tse, Nuclear spin-lattice relaxation via paramagnetic centers, Phys. Rev. 166 (1968) 279–291.

[46] N.A. Lin, S.R. Hartmann, Nuclear spin-lattice relaxation in CaF_2 via paramagnetic centers for short correlation time when spin diffusion is inhibited, Phys. Rev. B 8 (1973) 4079–4085.

[47] A. Abragam, Principles of Nuclear Magnetic Resonance, Oxford University Press, Oxford, 1961.

[48] Y. Zhou, B.E. Bowler, G.R. Eaton, S.S. Eaton, Electronspin lattice relaxation rates for S = 1/2 molecular species in glassy matrices or magnetically dilute solids at temperatures between 10 and 300 K, J. Magn. Reson. 139 (1999) 165–174.

[49] V. Ratner, E. Kahana, M. Eichler, E. Haas, A general strategy for site-specific double labeling of globular proteins for kinetic FRET studies, Bioconjug. Chem. 13 (2002) 1163–1170.

[50] K. Rang, Jan Sandström, C. Svensson, The conformational equilibrium of N,N'-bis[(S)-1-phenylethyl]-thiourea and its solvent dependence, studied by NMR and CD spectra and by X-ray crystallography, Can. J. Chem. 76 (1998) 811–820.

[51] S.S. Eaton, J. Harbridge, G.A. Rinard, G.R. Eaton, R.T. Weber, Frequency dependence of electron spin relaxation for three S = 1/2 species doped into diamagnetic solid hosts, Appl. Magn. Reson. 20 (2001) 151–157.